Bulletin of the Seismological Society of America, Vol. 99, No. 3, pp. 1853–1867, June 2009, doi: 10.1785/0120080244

Source Parameters for the 28 April 2007 M_w 4.0 Earthquake in Folkestone, United Kingdom

by L. Ottemöller, B. Baptie, and N. J. P. Smith

Abstract A moderate size earthquake (M_L 4.3, M_w 4.0) occurred in southeastern England on 28 April 2007. The earthquake was of some significance as it caused damage in the town of Folkestone and produced the largest peak horizontal ground acceleration (PGA, 0.1g) measured in the United Kingdom to date. It was followed by 12 aftershocks between M_L 0.8 and 1.7. The earthquake was the first of this size recorded by a significant number of newly installed broadband stations in the United Kingdom. The hypocenter of the event was at a depth of about 5 km beneath Folkestone, with an error ellipse indicating horizontal errors in a location of about 5 km. The depth was well constrained using a number of techniques, of which local travel-time inversion and teleseismic depth phase modelling are most reliable. A stress drop of 28.6 bars and a source radius of 0.5 km were determined from the analysis of displacement source spectra. We derived a near-surface attenuation factor $\kappa = 0.02$ from the aftershock data that were used in the spectral analysis of the mainshock. Applying the horizontal to vertical (H/V) spectral ratio technique to microtremor data recorded at a station 2 km from the epicenter revealed site amplification at frequencies of 0.4 and 3.9 Hz. This amplification is likely to have contributed to the mainshock PGA of 0.1g measured at the same site. Similar site conditions may have been responsible for the damage in parts of Folkestone. The moment tensor computed from regional broadband data showed a strike-slip mechanism with a normal component and either right-lateral movement on a west-southwest–east-northeast-striking or left-lateral movement on a north-northwest–south-southeast-striking nodal plane. The north-northwest–south-southeast-striking nodal plane matches the trend of the main faults affecting the Kent coalfield and also possibly the Variscan front. It is thus possible that the causative fault was associated with the Variscan front, a major structural boundary at the northern limit of late Carboniferous folding and thrusting.

Introduction

An earthquake of local magnitude M_L 4.3 occurred beneath the town of Folkestone, southeast United Kingdom, on 28 April 2007 at 07:18 coordinated universal time (UTC). The earthquake was strongly felt in Folkestone, where it caused minor damage. The earthquake was also felt further away across southeastern England. The earthquake was followed by 12 aftershocks, the last of which was on 5 May 2007. The largest aftershock had a magnitude of M_L 1.7. Details of a macroseismic survey and damage survey can be found in Sargeant *et al.* (2008), who estimate that the macroseismic intensity of the event was as large as VI on the European Macroseismic Scale. Damage mostly occurred in the Foord district of Folkestone and typically involved chimney collapse and narrow cracks in brick masonry walls (Sargeant *et al.*, 2008). Data from a strong-motion instrument, not located on bedrock and about 5 km from the hypocenter, suggest that the peak horizontal ground acceleration (PGA) may have been as large as 0.1g. The most damaging historical United Kingdom earthquake, M_L 4.6, occurred about 80 km north–northwest of Folkestone near Colchester in 1884.

Statistically, earthquakes of this size and greater occur in the United Kingdom every 4 yr (Musson, 1994). The largest previous earthquake to occur onshore in the United Kingdom was an M_L 4.7 earthquake near Dudley, West Midlands, in 2002 (Baptie *et al.*, 2005). While no previous earthquakes had been detected near Folkestone in instrumental times (since 1970) and seismicity is generally low in this part of the United Kingdom (Fig. 1), a few historic earthquakes are known to have occurred in the Dover Straits (Melville *et al.*, 1996). Worth mentioning are an M_L 5.8 earthquake in 1382, an M_L 5.8 in 1580, and an M_L 4.1 in 1776 (Musson,

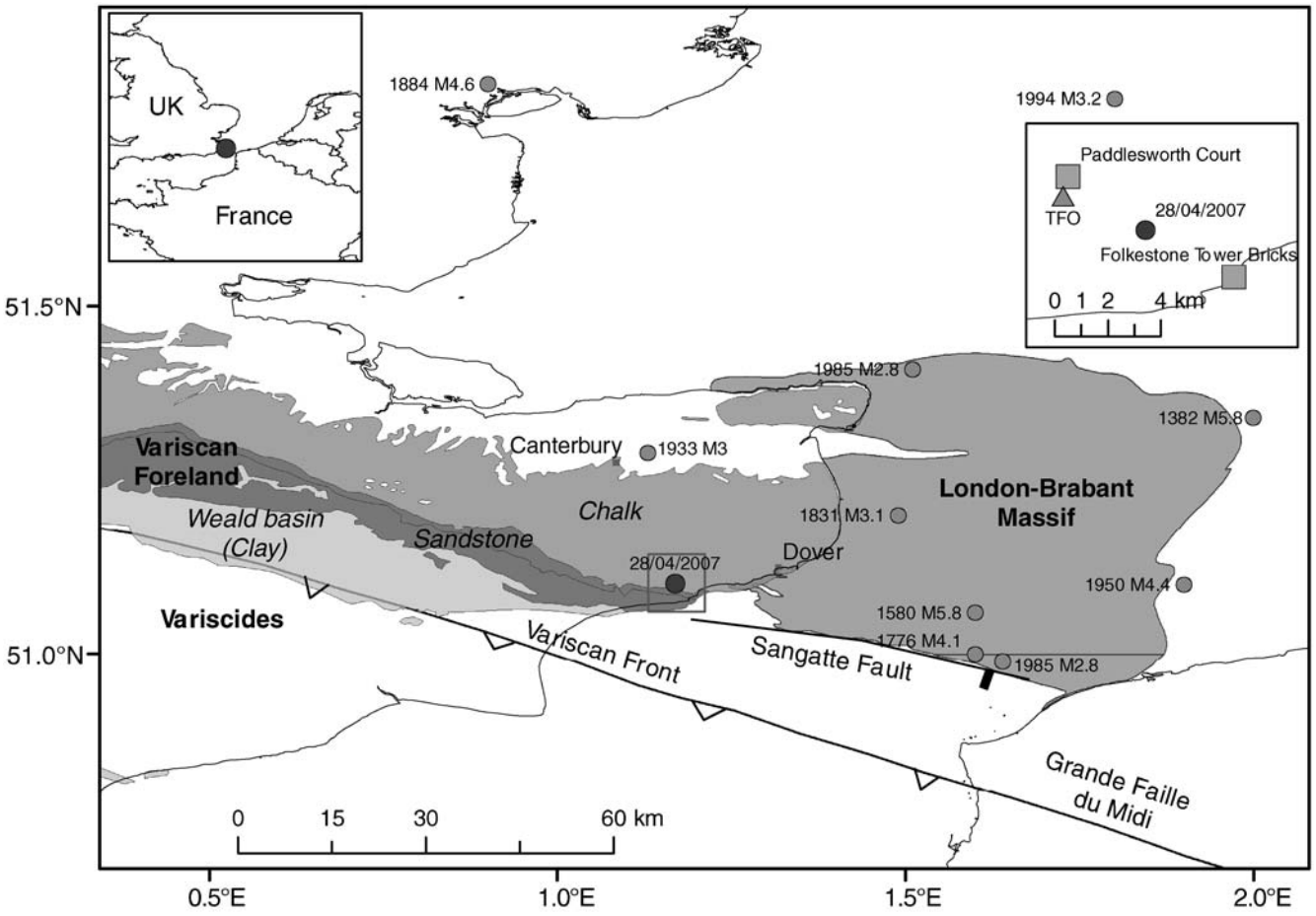

Figure 1. Simplified tectonic map for the area around Folkestone. The epicentral locations of the Folkestone earthquake and earthquakes with $M_L \geq 2.5$ are given by circles. The inset map in the top right corner gives the location of the two boreholes (square) mentioned in the text, and the location of the station at TFO (triangle) in relation to the epicenter (circle). The location of this map is indicated by a box around the epicenter on the main map. Symbols indicate the dip direction for the reverse fault Variscan front and the normal Sangatte fault.

1994, Fig. 1). The epicenters of these events are believed to be offshore, more than 30 km east of Folkestone, and, therefore, are attributed to a different source than the 2007 earthquake.

The United Kingdom seismic network operated by the British Geological Survey (BGS) previously comprised 146 short-period seismographs. Currently the network is being upgraded with the installation of broadband seismometers at a number of sites. At the time of the Folkestone earthquake a total of 15 permanent broadband stations (12 operated by the BGS, two by Atomic Weapons Establishment [AWE] Blacknest, and one by the Incorporated Research Institutions for Seismology [IRIS]) were operational in the United Kingdom. This event is, therefore, one of the first events in the United Kingdom above an M_L 4 recorded on a significant number of broadband stations. Here we utilize these high quality data in the analysis of the earthquake. Just as important, both short-period and broadband seismic data were available from continental Europe. Two temporary stations were deployed by the BGS to record aftershocks. However, these were only in place for the last of the 12 aftershocks.

In this article we describe the analysis of all seismic data available to us from the Folkestone earthquake to: (1) determine the hypocenter location and magnitude; (2) determine the source radius and stress drop from spectral analysis; (3) use the H/V spectral ratio technique to estimate amplification at the site in Folkestone; (4) determine the source mechanism through moment tensor inversion; (5) estimate the depth through modelling of teleseismic depth phases; (6) estimate the depth through local waveform modelling; and (7) attempt to understand the event within the tectonic context. This understanding of the earthquake source can be the basis of future studies into the observed ground motion and damage in the source area.

Tectonics and Crustal Velocity Model

Tectonic Overview

The port of Folkestone is situated within the county of Kent on the southeast coast of England. Figure 1 presents an overview of the tectonics around the epicenter in Folkestone. Geologically, Folkestone lies on the northeast margin of the

Mesozoic Weald Basin (Lamplugh *et al.*, 1923) and is underlain by the Kent coalfield (depth 0.3–1.5 km). The coalfield occupies a Carboniferous basin with its northwest–southeast trending depocenter coinciding with a southeast-plunging syncline (Dines, 1933) that reaches the coast east of Dover. The Variscan front is a concealed southwest-dipping thrust fault at the northern limit of late Carboniferous folding and thrusting, and it bounds the Kent coalfield to the south. It also probably forms the northeastern marginal faults of the Weald Basin and is traditionally placed along the Grande Faille du Midi in northern France (Bouroz, 1962). North of the Variscan front is the London–Brabant Massif, a topographic high that was above sea level during most of the Carboniferous folding and thrusting. Caledonian faults of northwest–southeast trend and prelate Devonian age are expected to be present in the basement of the Massif, but have not been clearly mapped.

From work in the offshore area to the south (Warren and Harris, 1996) it is clear that another Carboniferous syncline was formed southwest of the southeast-plunging syncline with two intervening folds, one anticlinal and the other monoclinal. Synclinal reflectors of Carboniferous age terminate at an east–west fault that appears to be that shown by Minguely *et al.* (2005) heading toward France and called the Sangatte fault. It may control the Tertiary Quenocs Anticline (Bureau de recherches géologiques et minière [BRGM], 1971), forming the southern limit of the Cretaceous chalk on the sea floor. Other folds affecting the chalk trend approximately east–west (Shephard-Thorn *et al.*, 1972; Auffret and Colbeaux, 1977).

Faulting

Mesozoic faults in the Weald Basin are typically of early to late Jurassic age, dip south, and act as syn-sedimentary growth faults (tilting basement blocks northward). Many appear to have been rejuvenated from Variscan thrusts and were also reactivated in Tertiary times as reverse faults. Mainly northwest–southeast faults affect the Mesozoic strata above the Kent coalfield (Plumptre, 1959).

A northwest-trending fault was mapped as the boundary between two Variscan blocks during the Channel Tunnel investigations and was described as connecting southeast to the Sangatte fault (Warren and Harris, 1996). Warren and Harris (1996) show that the fault probably dips west, down-faulting in this direction during the deposition of Gault and Lower Chalk. The fault affects Jurassic deposition, which probably means that it reaches at least below the depth of the Variscan unconformity and is assumed to continue downward. We identify this structure as the closest fault to the Folkestone earthquake. The Sangatte fault with an east–southeast trend was mapped by Minguely *et al.* (2005). It may terminate the Carboniferous syncline to the south and is probably a thrust, but lies northeast of the traditionally located position of the Variscan front between England and France (Fig. 1).

Velocity Model

A number of regional velocity models derived from seismic refraction surveys are being used at the BGS for locating earthquakes in the United Kingdom (Booth *et al.*, 2001). In the absence of a specific velocity model for southeast England, initial locations were determined using a default United Kingdom model. However, this was insufficient to explain both the near-source and distant arrival time observations. Therefore, we constructed a velocity model appropriate for the vicinity of Folkestone that is consistent with the shallow structure around Folkestone as well as the deeper regional structure.

In the Folkestone area at least the top 5 km are likely to be of sedimentary origin (Fig. 2). The depth of formations down to the top of the Carboniferous limestone is based on the Paddlesworth Court borehole (BGS Reg. No. TR14SE3) and the Folkestone Tower Brickworks borehole (BGS Reg. No. TR23NW38). The sequence is only reliably known down to this level, but a deeper section using boreholes in the surrounding area has been compiled.

The *P*-wave velocities of the main Mesozoic formations and coal measures were derived from Kent coalfield boreholes. The Mesozoic formations show thickening to the

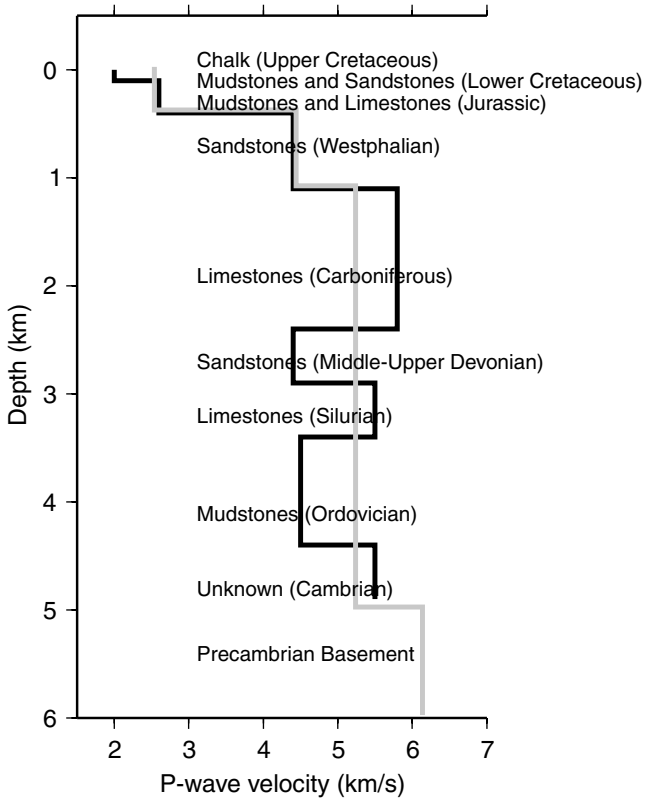

Figure 2. Shallow *P*-wave velocity model for Folkestone. The black line gives detailed velocities as explained in the main text. The gray line gives the model simplified through the averaging of the detailed model that is used to locate the hypocenters. Lower Cretaceous and Jurassic are condensed formations, underlain by Palaeozoic formations.

southwest, toward the Weald Basin. The coal measures extend at least as far south as the Sangatte fault (offshore), and a greater thickness is preserved in the syncline northeast of Folkestone.

The thickness of the Carboniferous limestone is taken from an interpretation of the nearest available seismic reflection profile offshore in the Dover Strait. Boreholes within the Kent coalfield show that coal measures lie unconformably on Carboniferous limestone strata with a *P*-wave velocity of 5800 m/sec. Limestones and dolomites, responsible for higher velocities observed elsewhere in southern England (Smith *et al.*, 2001), have been eroded in Kent. Identification of Devonian and deeper formations are more speculative.

Less is known about the deeper structures in southeastern England, and in the absence of specific studies we constructed two velocity models from regional models (Fig. 3). First, we built a velocity model combining the shallow structure (Fig. 2) with the structure from the CRUST 2 model (Mooney *et al.*, 1998; Bassin *et al.*, 2000) for the epicentral location. Apart from the shallow structure, this model is not very different from models used for routine hypocenter locations (Booth *et al.*, 2001). Second, we extracted the velocity model near the hypocenter from the global surface wave tomography model of Shapiro and Ritzwoller (2002). We used this model to compute the Green's functions used in the moment tensor inversion. We assume the first model to be more appropriate near the source, which is important for calculating travel times near the source, and the second model better for computing regional surface waves.

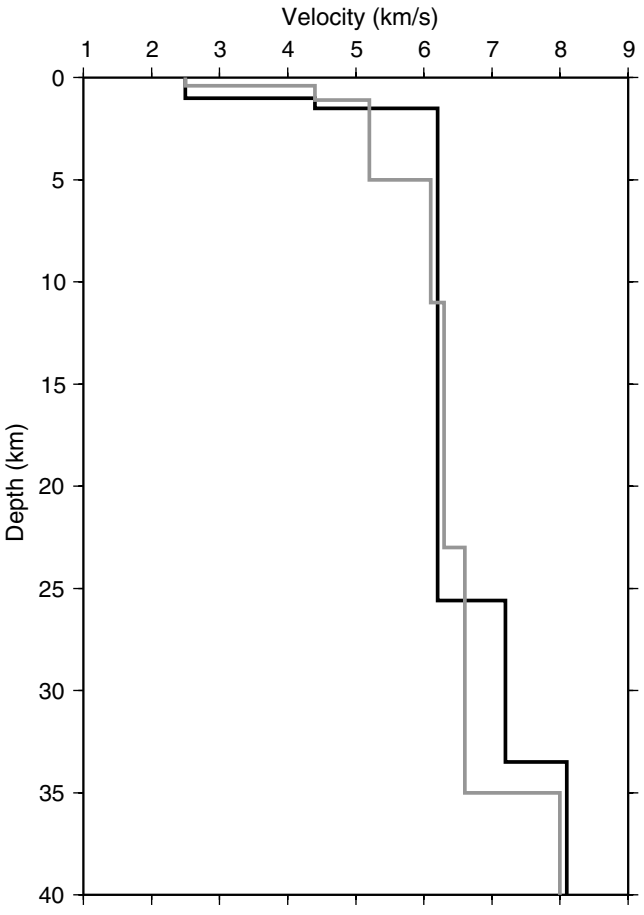

Figure 3. *P*-wave velocity models used for hypocenter location (gray) and moment tensor inversion (black).

Hypocenter Location from Travel-Time Inversion

The earthquake was well recorded on seismic stations across the United Kingdom, and also across western Europe from Norway to Spain (Fig. 4). The nearest recording station was TFO (Folkestone), only a few kilometers outside Folkestone and 2 km from the epicenter. We measured *P*-wave arrival times from vertical-component data and *S*-wave arrival times from horizontal-component data where possible (Fig. 4). The hypocentral location was computed using the HYPOCENTER program (Lienert, 1994; Lienert and Havskov, 1995) that performs a standard linearized least-squares inversion based on a 1D velocity model (Fig. 3). We applied a distance weighting where the weight is linearly reduced from one at a distance given by *x*near to zero at a distance given by *x*far. The values chosen were *x*near = 200 km and *x*far = 400 km, which was a compromise between using the nearest stations only and minimizing the azimuthal gap (Fig. 4a). Applying this distance weighting, a total of 35 *P*- and 12 *S*-wave arrivals were used. Figure 5a shows that as expected, the residuals are smaller for stations within *x*near. It also shows that for most stations beyond *x*near, the observed travel time is less than the calculated travel time, as they are weighted less due to the trade-off between origin time and travel times.

The results from the hypocenter determination are given in Table 1. Figure 4b shows the computed 90% error ellipse, which demonstrates that the solution is best constrained in a northwest–southeast direction as expected from the station distribution. The computed horizontal errors are of the order of 5 km, which is similar to errors computed for the recent Buncefield explosion where the source location was known and covered by the error ellipse (Ottemöller and Evers, 2008). The solution is slightly east of the solution given by the U.S. Geological Survey (USGS) National Earthquake Information Center (NEIC) based on a global velocity model. We consider our solution to be better, as it is based on more local stations and a local velocity model. However, it is interesting to note that the location ellipse based on a global model overlaps with the error ellipse from local data.

The hypocentral depth was estimated at 5.3 km with an uncertainty of ±4 km. In addition, the root mean square residual (rms) versus depth plot (Fig. 5b, with 1 km spacing) shows that there is a global minimum at 6 km. Generally, depth determination requires a station with an epicentral distance of less than twice the event depth, which is the case here, and the depth error is probably overestimated.

The average time between *P*- and *S*-wave arrivals at the nearest station was measured for the mainshock and

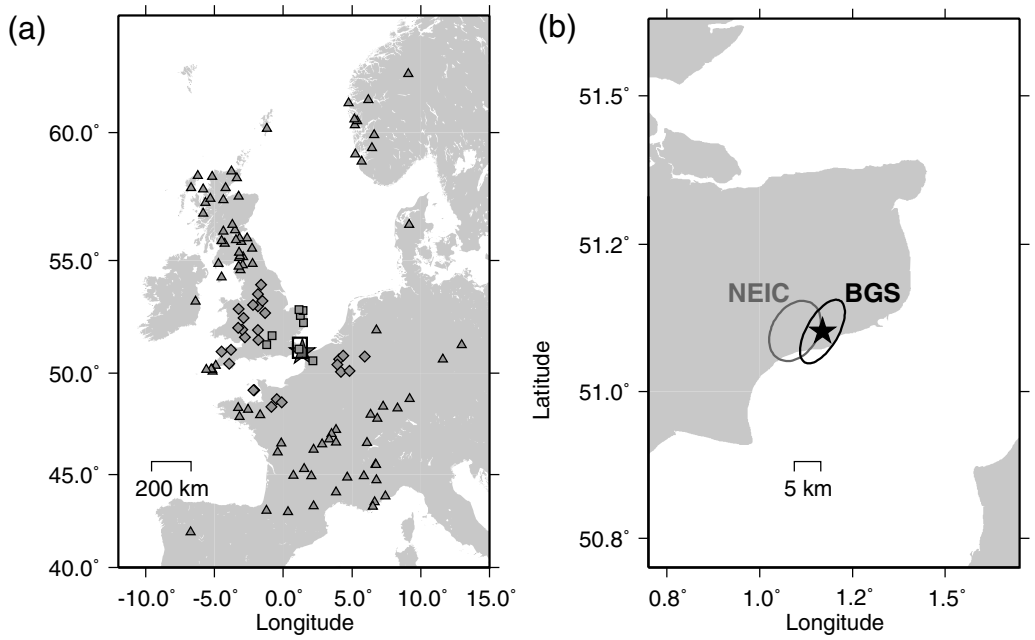

Figure 4. Station distribution and error ellipses: (a) Map of stations with picked arrival times where squares are stations within distance *x*near, diamonds are stations within distance *x*far, and triangles give stations with arrival times that are not used to determine the hypocenter; (b) Error ellipse (90% confidence) computed using the stations shown in (a) BGS and ellipse given by the USGS NEIC using a global velocity model.

aftershocks as $t_s - t_p = 0.86$ sec ± 0.17. This standard deviation equates to about a 1 km change in hypocenter location. The aftershock on 5 May at 05:09:18 is the only event for which data were recorded on two temporary stations in addition to TFO, and thus, the only of the 12 aftershocks that could be located. The location determined with the three stations for this event is shifted by 2.2 km to the east and 0.3 km to the south, and the depth is 1.7 km more shallow than the mainshock. The computed change is larger than suggested by $t_s - t_p = 0.9$ sec, which is not unexpected as the hypocenters are not computed jointly. We assume that the aftershocks are located within about 1 km of the mainshock, and for magnitude computation and spectral analysis fix the aftershock locations to that of the mainshock. Comparing the aftershock waveforms, we can identify three groups of similar events with a cross-correlation greater than 0.8 of four, four, and three events, respectively. Observing the three event groups suggests that the aftershocks do not all have the same mechanism and are at least partly different from the mainshock. However, the aftershock recordings cannot be

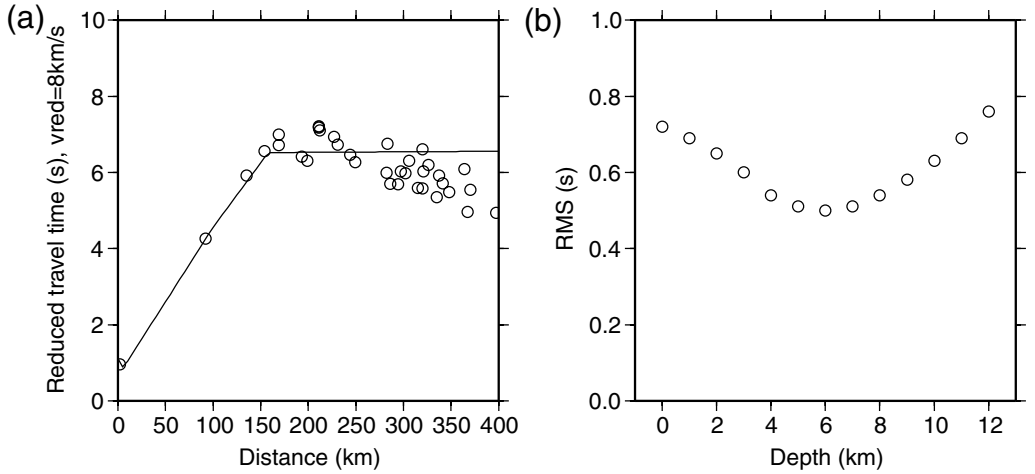

Figure 5. Results from the hypocenter location using the local model (Fig. 3) and distance weighting parameters of *x*near = 200 km and *x*far = 400 km: (a) reduced *P*-wave travel times as a function of distance; observed times are given by circles and calculated times by the solid line. (b) computed rms as a function of depth, determined by inverting time for origin and epicenter for fixed depth.

Table 1
Results from Hypocenter Location

Parameter	Value
Date and Time	28/04/2007 07:18:11.4 ±1.6 sec (UTC)
Latitude	51.102°N ± 4.6 km
Longitude	1.169°E ± 6.1 km
Depth	5.3 ± 4 km
RMS	0.5 sec
Azimuthal Gap	86°
Error Ellipse (smajor/ sminor/azimuth)	6.7 km/3.0 km/29.7°

compared to the saturated data from the mainshock, and no significant further conclusions can be drawn.

Magnitude and Spectral-Source Parameters

In this section we determine the magnitude of the mainshock and aftershocks. We also derive near-surface attenuation from the aftershocks and use that to determine source size and static stress drop of the mainshock.

Local Magnitude M_L

An M_L 4.3 was computed for the mainshock as the average of estimates derived from the largest *S*-wave amplitudes at 21 stations in the distance range 169 to 1017 km. The amplitudes were measured on horizontal component-simulated Wood–Anderson records. The M_L formula derived for California (Hutton and Boore, 1987) is still the default used in the United Kingdom

$$M_L = \log(A) + 1.11\log(D) + 0.00189 \times D - 2.09, \quad (1)$$

where the amplitude (A) is in newton meters and the distance (D) in kilometers.

For the aftershocks the magnitudes were determined by assuming that they were colocated with the mainshock. Horizontal maximum amplitudes were measured on the nearest station TFO only, as only one aftershock was recorded on additional stations. This allows for a relative comparison of aftershock magnitudes, if we ignore the possibility that they have different mechanisms that lead to a variation in radiation pattern and observed amplitudes. Figure 6 shows the magnitude distribution of mainshock and aftershocks with time. Aftershock magnitudes are in the range M_L 0.8–1.7, and thus, the largest aftershock is 2.6 magnitude units smaller than the mainshock. The two largest aftershocks (both M_L 1.7) occurred within about four hours of the mainshock.

Analysis of Source Spectra

The earthquake source spectrum $S(f)$ is often approximated by the ω^2 model (Aki, 1967; Brune, 1970). The observed displacement spectrum after correcting for instrumentation is given by

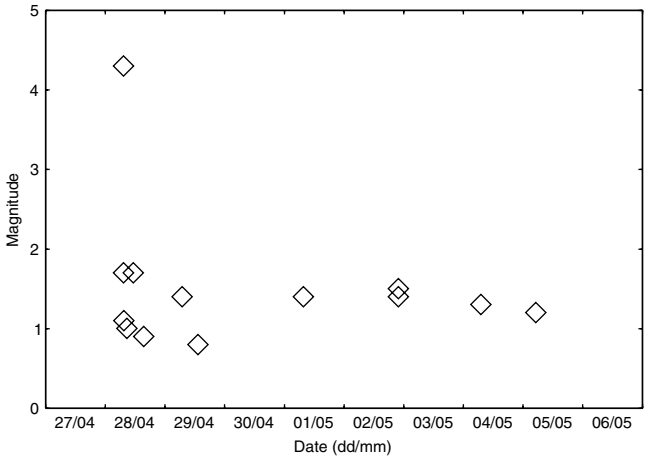

Figure 6. Aftershocks plotted by magnitude versus origin time.

$$A(f) = G \times M_0 \times 2.0 \times 0.6 \times S(f) \times D(f), \quad (2)$$

where G describes geometrical spreading, M_0 is the seismic moment, and the factors 2.0 and 0.6 account for radiation. The correction for attenuation $D(f)$ is commonly constructed in two parts. The first correction accounts for attenuation along the path described by $Q(f)$ and the second accounts for near-surface attenuation κ near the receiver (Singh *et al.*, 1982).

$$D(f) = \exp\left[\frac{-\pi T f}{Q(f)}\right]\exp(-\pi\kappa f), \quad (3)$$

where T is travel time. We used the United Kingdom average attenuation model of (Sargeant and Ottemöller, unpublished manuscript, 2007)

$$Q(f) = 335\left[\frac{f}{1.58}\right]^{0.45}. \quad (4)$$

The near-surface attenuation can be determined from records at short hypocentral distance, where path attenuation is not significant. For frequencies below the corner frequency of an event κ can be determined from the slope of the displacement spectrum, that when corrected for attenuation, is expected to be flat. For this analysis we selected Folkestone aftershocks that are small enough to have a corner frequency higher than the maximum frequency in our analysis of 5–20 Hz. From the equations for stress drop ($\sigma = 0.44M_0/R^3$) and source radius ($R = 0.35v_s/f_c$), assuming a stress drop of 30 bars, we find that an M_W 1.7 event may be expected to have a corner frequency of 30 Hz. To exclude saturated records we use the more conservative maximum magnitude M_L 1.5, and assume $M_L = M_w$. Using these criteria and data from 10 aftershocks we get $\kappa = 0.02 \pm 0.01$. This value lies between observed κ values of 0.05 in California (e.g., Abercrombie, 1997) and hard-rock sites where $\kappa = 0.005$ (e.g., Atkinson and Boore,

2006), and appears to be reasonable for this site on top of sedimentary rocks.

We now use this κ value and $Q(f)$ as given in equation (4) to determine the seismic moment, corner frequency, and stress drop for the mainshock using the method of Ottemöller and Havskov (2003). The data comprise seven vertical-component broadband records from a distance range of 169 to 402 km. We use the same κ for all stations, although strictly this is derived for station TFO only. The results are $M_0 = 5.7 \times 10^{14}$ Nm, $M_W = 3.8 \pm 0.1$, $f_c = 2.6$ Hz $\pm$ 0.7, $R = 0.5$ km $\pm$ 0.1, and $\sigma = 28.6$ bars $\pm$ 24 (we exclude the low and high extreme values when averaging f_c, R, and σ). This analysis is not performed for the aftershocks, as the corner frequency is too close to the Nyquist frequency and f_c would not be determined correctly.

PGA and Site Effects

The PGA measured from the Folkestone earthquake reached 0.1g at a distance of about 5 km and is the highest ever recorded in the United Kingdom. The PGA time series plot (Fig. 7) shows that the highest values were observed on the horizontal components. The largest amplitudes were reached over one cycle with a period of 0.07 sec, corresponding to 14.3 Hz. The accelerograph was configured to record up to 0.1g, which was exceeded in this case on both horizontal components. The data were thus clipped for a few samples, which needs to be considered when processing the data. Here we use the Nakamura or horizontal to vertical (H/V) spectral ratio technique (Noghoshi and Igarashi, 1970, 1971; Nakamura, 1989) to empirically estimate the site response. The technique involves computation of the H/V spectral ratio from microtremor recordings. The peaks in the H/V ratio are related to sharp impedance contrasts below the recording site. This technique is expected to reveal the fundamental frequencies at which amplification occurs but not with the correct amplitudes (e.g., Atakan *et al.*, 2004b; SESAME, 2004). While there are limitations to this method, a great number of field studies suggest that it works (e.g., Konno and Ohmachi, 1998; Sørensen *et al.*, 2006).

We used microtremor recordings at the station TFO, the recording site nearest to the earthquake, to compute the H/V spectral ratio. The site was equipped with a Willmore short-period seismometer with a natural period of 1 sec. A total of 86 time windows of 40 sec duration were used for a seven day period in the beginning of October 2007. The spectra were smoothed using the function suggested by Konno and Ohmachi (1998) applying a coefficient for bandwidth of 20.

The resulting H/V ratio curve (Fig. 8) shows two peaks at 0.4 and 3.9 Hz that are clear according to the SESAME (2004) guidelines. There is a smaller, less significant peak at 17 Hz. This frequency coincides with the frequency of the mainshock horizontal PGA. A simple relationship states that the depth of the impedance contrast (h) is related to the S-wave velocity above (V_S) and frequency of amplification (f) by (e.g., SESAME, 2004)

$$h \approx V_S/(4 \times f). \tag{5}$$

The site geology at TFO consists of near-surface clay with flints overlying the chalk. Although the near-surface geology at TFO is unknown in detail, nearby boreholes suggest a thickness of the superficial sediments of 2–18 m with a density-derived (Nafe and Drake, 1963) V_S of about

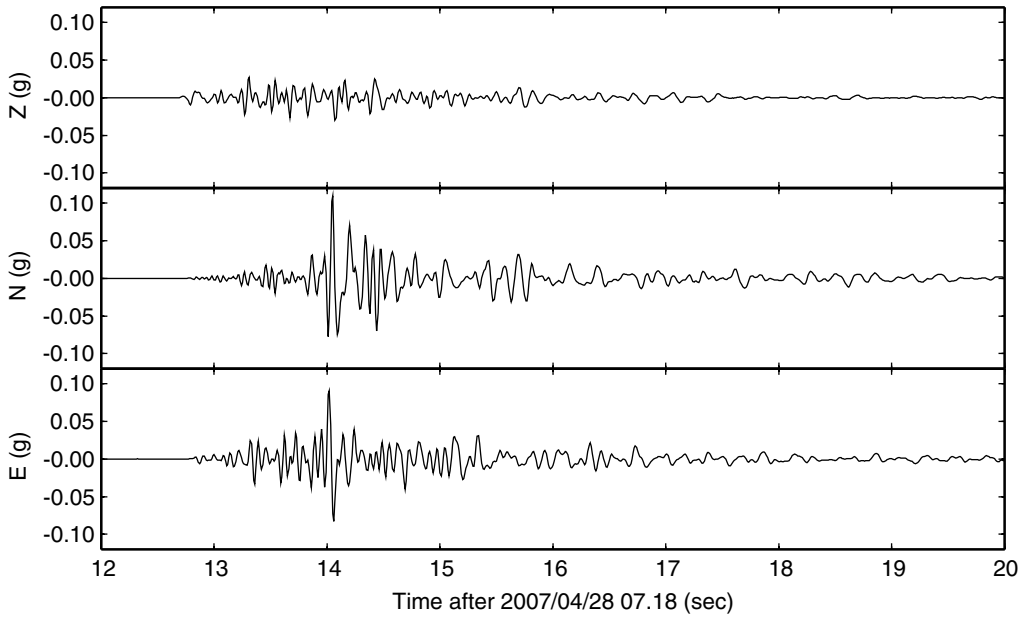

Figure 7. Acceleration observed on an accelerometer at station TFO. Note that the instrument clipped at 0.1g.

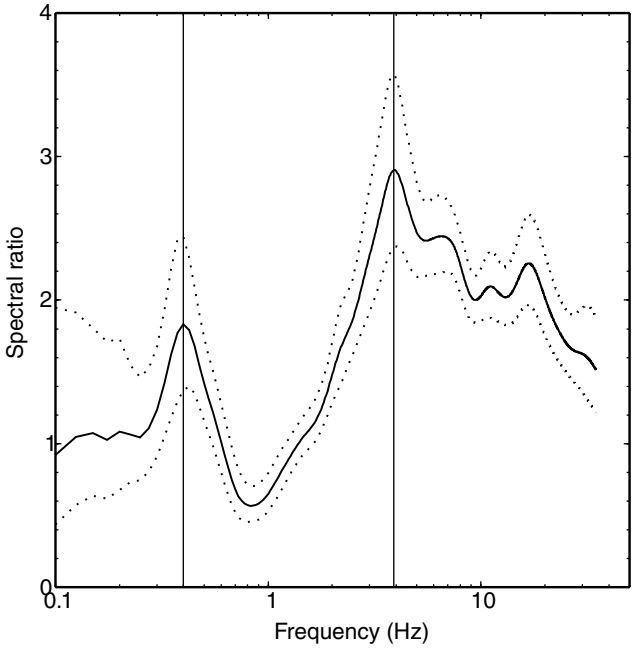

Figure 8. Spectral ratio of H/V-component ambient noise measurements at station TFO. The dotted lines indicate $\pm 1\sigma$.

750 m/sec. The peak at 17 Hz is related to an impedance contrast in the top few meters (11 m according to equation 5), possibly at the base of the superficial sediments. Assuming a V_S of 1 km/sec below the surface sediments (approximate average between velocities above and below), the 3.9 Hz peak corresponds to an impedance contrast at a depth of about 70 m. Assuming an average V_S of 1.4 km/sec at greater depth (Fig. 2), the peak at 0.4 Hz corresponds to a contrast at about 900 m depth. Compared with our shallow velocity model used for hypocenter location, the two impedance contrasts may correlate with the base of Upper Cretaceous and Westphalian, respectively. However, without more detailed knowledge of the site geology this interpretation remains uncertain.

Source Mechanism from Moment Tensor Inversion

Moment tensors are routinely calculated for moderate sized earthquakes and are often considered in seismotectonic interpretation. Recent moment tensor solutions computed in and around the United Kingdom include the Dudley earthquake in 2002 (Baptie *et al.*, 2005) and the induced Ekofisk event in 2001 (Ottemöller *et al.*, 2005). The Folkestone mainshock was well recorded by seismic broadband stations in the United Kingdom and across Europe (Fig. 9). Signal energy at long periods was sufficient to perform moment tensor inversion that was undertaken using the software of Dreger (2003), developed and routinely used at the University of California, Berkley Seismological Laboratory. Full regional waveforms were used and synthetic waveforms were computed for a 1D velocity model. The moment tensor was determined through linear least-squares inversion following Jost and Herrmann (1989) and decomposed into double-couple and compensated linear vector dipole components. Stations and components (either one, two, or three) were manually selected based on the signal-to-noise ratio. Stations northeast of the epicenter in Denmark and Norway could not be used due to noisy signals, possibly related to high attenuation in the North Sea region. Data were band-pass filtered in the period range 15–40 sec. The synthetics were computed based on a 1D velocity model (Fig. 3) not accounting for lateral variations that works because the waveforms are not very sensitive to the model at long periods.

While the moment tensor inversion is sensitive to depth, depth determination is not part of the inversion. However, a common approach is to invert the moment tensor for a range of hypocentral depths to test which depth gives the lowest variance (e.g., Braunmiller *et al.*, 2002; Dahm *et al.*, 2007). We inverted for depths between 1 and 12 km (Fig. 10) and found the lowest variance for a depth of 3 km. The moment tensor obtained for 3 km depth, therefore, is our preferred solution (Fig. 11). A good match between observed and calculated waveforms is obtained (Fig. 12).

The solution obtained shows predominantly strike-slip faulting with a normal component. Fault slip was either right-lateral on a west-southwest–east-northeast-striking, or left-lateral on a north-northwest–south-southeast-striking nodal plane. The double-couple component of the moment tensor is 93%. The difference between the obtained moment tensor solutions for the various depths is not very significant. We also obtained similar results when using different velocity models such as the Preliminary Reference Earth Model (PREM) or the United Kingdom average model, and when using stations in the United Kingdom only, which showed that the solution is robust.

Waveform Modelling

The source depth is reasonably well constrained through travel-time inversion due to the near-source station TFO, but less well constrained through moment tensor inversion. We now explore the use of waveform modelling as an independent means of constraining depth.

Depth phases such as pP observed at teleseismic distances are commonly used to determine source depth, because it is well known that the arrival time of pP relative to P is nearly independent of the velocity structure between source and receiver, depending only on the velocity structure above the source. We follow a similar approach to Dahm *et al.* (2007) and use two different methods to constrain the source depth: (1) identifying and modelling pP observed at teleseismic distances; and (2) waveform modelling of the observations at the closest stations. Both modelling procedures are based on the moment tensor determined in the previous section.

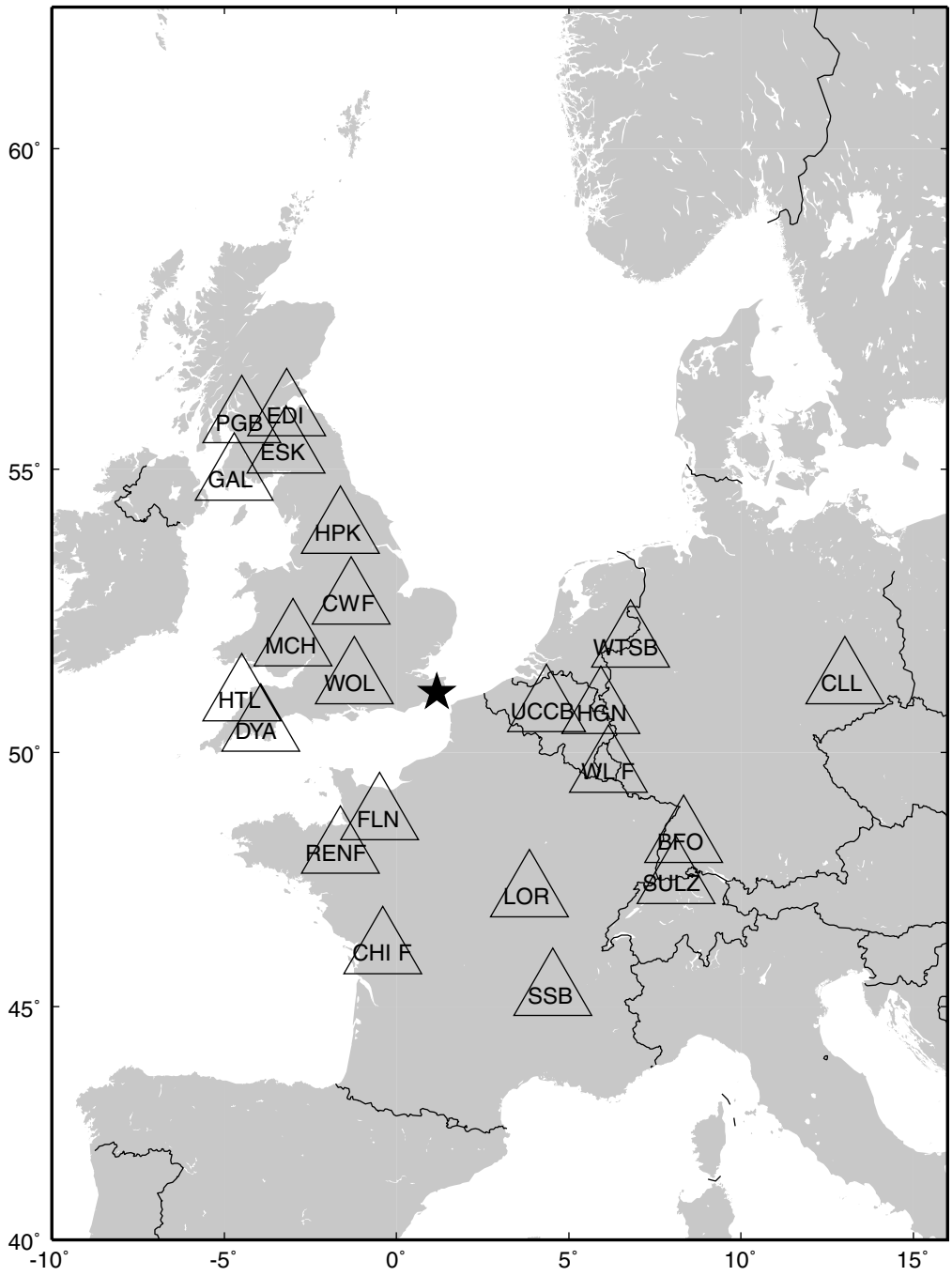

Figure 9. Map of broadband stations used for moment tensor inversion. The star indicates the epicenter.

Teleseismic Modelling

The Folkestone earthquake was well recorded on the Yellowknife array (YKA) in Canada (distance = 55.95°, azimuth = 329.7°) and also on the Makanchi array (MKAR) in Kazakhstan (distance = 50.91°, azimuth = 61.0°). We calculated beams for each array using the bearing and apparent velocity calculated from frequency wavenumber analysis of the *P*-wave arrival, which resulted in a significant improvement in signal-to-noise ratio.

To assist interpretation we used the method of Wang and Wang (2007) to calculate synthetic seismograms for an epicentral distance corresponding to YKA and MKAR that could be compared with the observed beam. The ak135-layered Earth velocity model (Engdahl *et al.*, 1998) was used, but our local near-source crustal velocity model (Fig. 2) was also incorporated. Source depth was varied between 1 and 10 km in 1 km steps. The source duration for the calculation was 1.0 sec. In addition the synthetic seismograms were

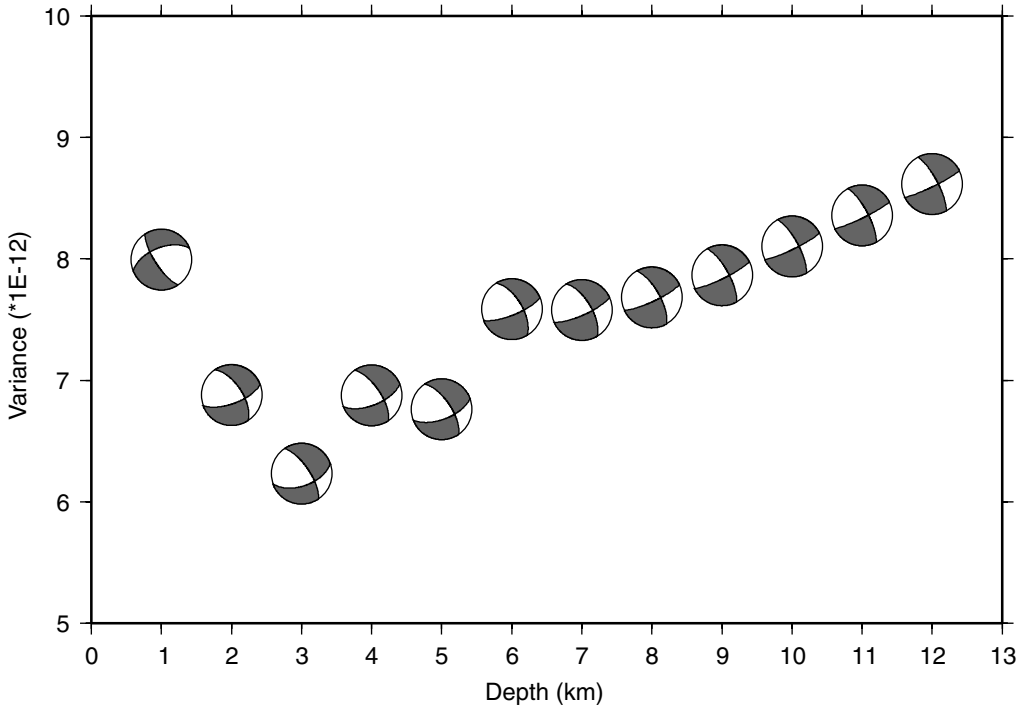

Figure 10. Variance in moment tensor inversion for range of fixed depths.

convolved with the instrument response of the short-period seismometers at both YKA and MKAR to allow direct comparison with the observed beam.

Comparison of the synthetics with the observed beam for both arrays (Fig. 13) shows a good match for a source depth of between 4 and 5 km, with a clearly observed pP phase at around 2 sec after the initial arrival. Using the ak135 model at both source and receiver results in only a small change to the calculated pP-P time, leading to a depth of between 5 and 6 km.

Modelling at Regional Distances

Depth phases observed at regional distances can also be used to constrain the source depth (Kind, 1979). In this case pPn/g or sPn/g is generally used. Here we compare observations of the Pn/g arrival at station WOL, located 169 km from the epicenter, with modelled Pn arrivals for source depths between 1 and 10 km. Synthetic seismograms were calculated using the discrete wavenumber integration method of Herrmann (1996) and the local velocity model used previously. Figure 14 shows both modelled and observed displacement seismograms at station WOL. The pPn/g phase can be clearly observed on the modelled seismograms as the source depth increases. For source depths between 4 and 10 km, the delay between P and pP is approximately 2–4 sec. By contrast the observed seismograms do not show a separated pP phase. Instead, we observe a slightly elongated pulse shape that might be indicative of a source depth of around 3 ± 2 km. It is clear that using local observations to constrain source depth is less conclusive than use of teleseismic data.

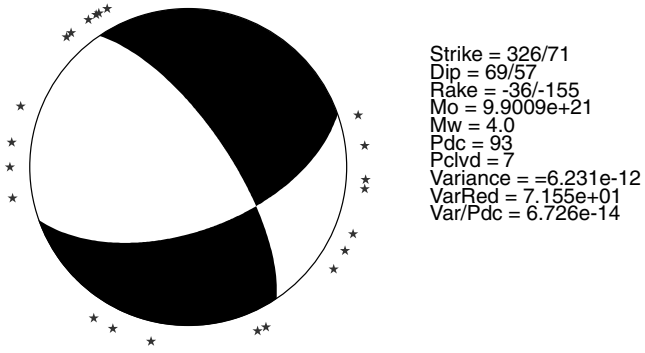

Figure 11. Moment tensor solution (lower hemisphere projection) for a source depth of 3 km. The stars indicate the azimuths of the stations used.

Interpretation and Discussion

The two main results obtained here are the hypocentral location and source mechanism. Knowledge of epicentral location and depth is important to determine the distance between the earthquake and the area of damage in Folkestone. The epicenter is well constrained due to good azimuthal station coverage and knowledge of the shallow velocity structure near the epicenter. The horizontal error (90% confidence) is of the order of 5 km. The depth was determined in a number of ways. From the local data, the depth was determined at 5.3 ± 4 km from travel-time

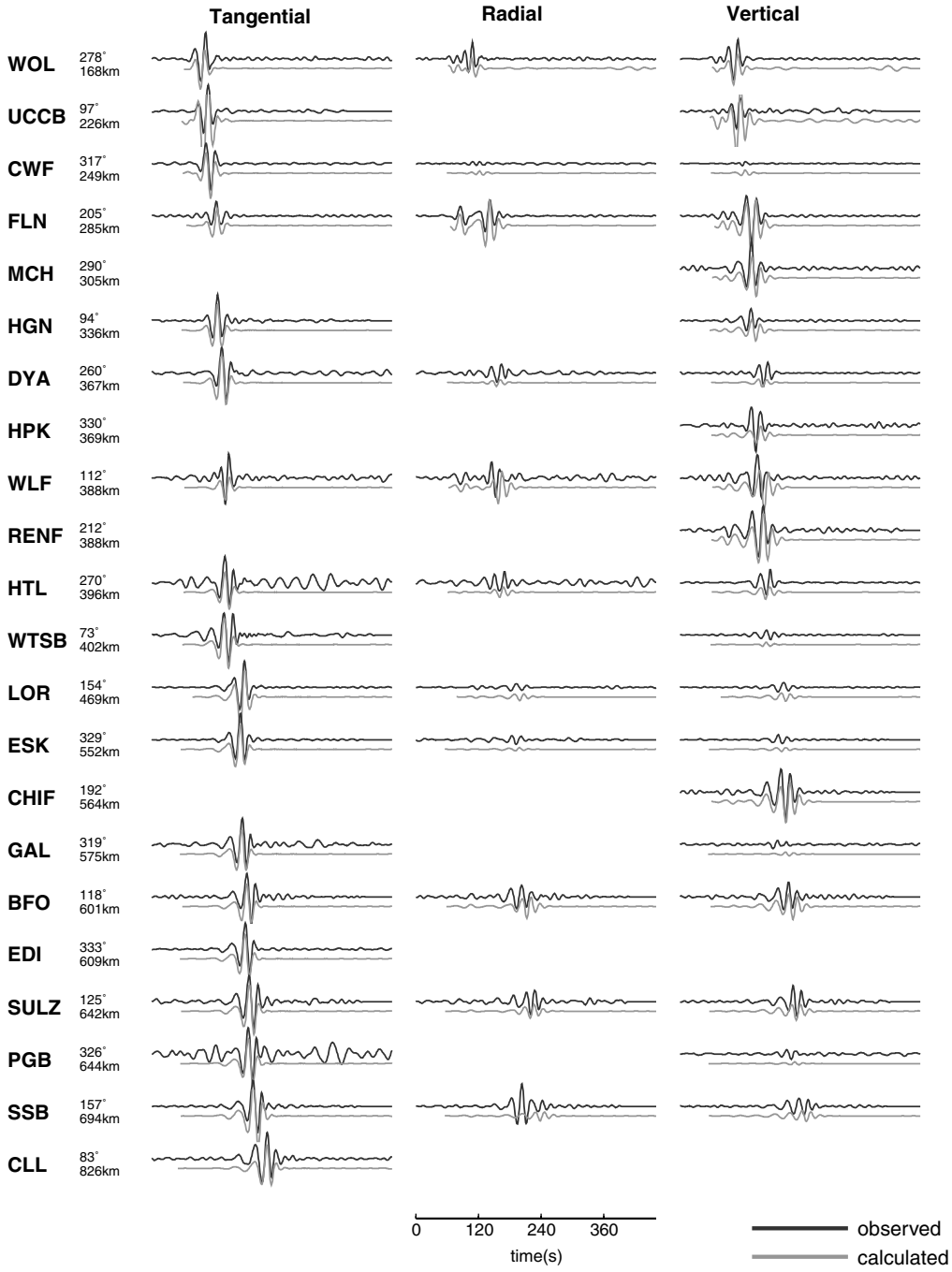

Figure 12. Comparison of observed (dotted black lines) and synthetic seismograms (solid gray lines) used in moment tensor solution for a source depth of 3 km.

inversion and at 3 ± 2 km from waveform modelling. From the moment tensor inversion using regional data we obtained the lowest variance for a depth of 3 km with an uncertainty of ± 2 km, corresponding to a 10% change in variance. The teleseismic modelling gives a depth of 4–5 km. Combining these results and considering that depth is better constrained by the travel time-inversion and teleseismic modelling, we conclude that the depth is best given as 5 ± 2 km. While the rocks at 5 km are not known with certainty, we assume that below 5 km the fault would be within the Precambrian.

The source mechanism was well resolved through moment tensor inversion using data from stations with good regional coverage. The solution was stable when inverting for different fixed source depths or using alternative velocity models. It was also independent of the station configuration, and within expected uncertainties the same solution was obtained using stations in the United Kingdom only.

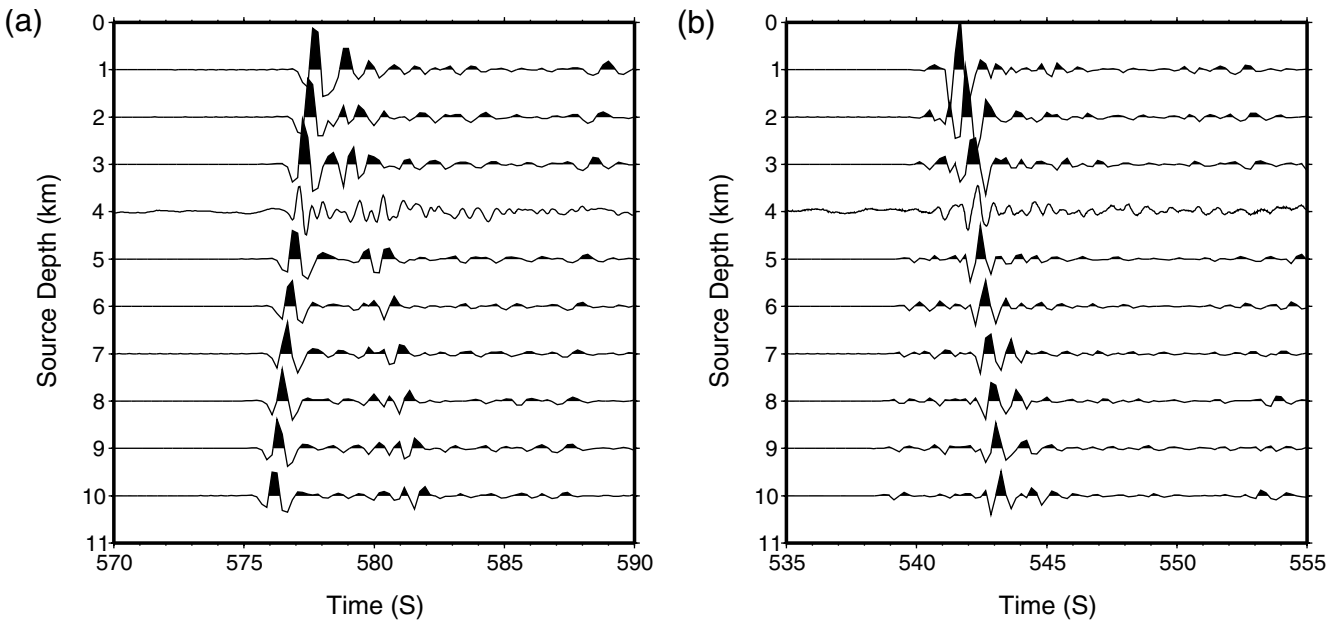

Figure 13. Synthetic seismograms calculated for (a) YKA and (b) MKAR using different source depths and a local velocity model at the source. The observed beams from frequency wavenumber analysis are shown at a source depth of 4 km. Times are relative to the origin time.

The solution obtained shows strike-slip faulting with a normal component. The two nodal planes indicate right-lateral movement with the fault striking west-southwest–east-northeast or left-lateral movement on a north-northwest–south-southeast-striking fault. The moment tensor gives no preference to one of the nodal planes, and other information would be required to choose a preferred solution. Unfortunately all but one of the aftershocks cannot be located and we are thus unable to infer the fault orientation. The axis of maximum compressive stress associated with the fault-plane solution points approximately east–west in agreement with the understanding of regional stresses related to the ridge-push force from the Mid-Atlantic (Davenport *et al.*, 1989; Baptie *et al.*, 2005).

As mentioned previously in this article, parts of the Variscan front strike northwest, and it may be more likely that our north–northwest-striking nodal plane is the causative fault. However, the west–southwest-striking fault plane cannot be ruled out, particularly considering that the source radius is only 0.5 km. There is considerable uncertainty on the exact course of the front in Kent. The southwestern part of the error ellipse probably covers the northernmost Variscan front thrust and its rejuvenated fault movement. However, there is a problem with the definition of the

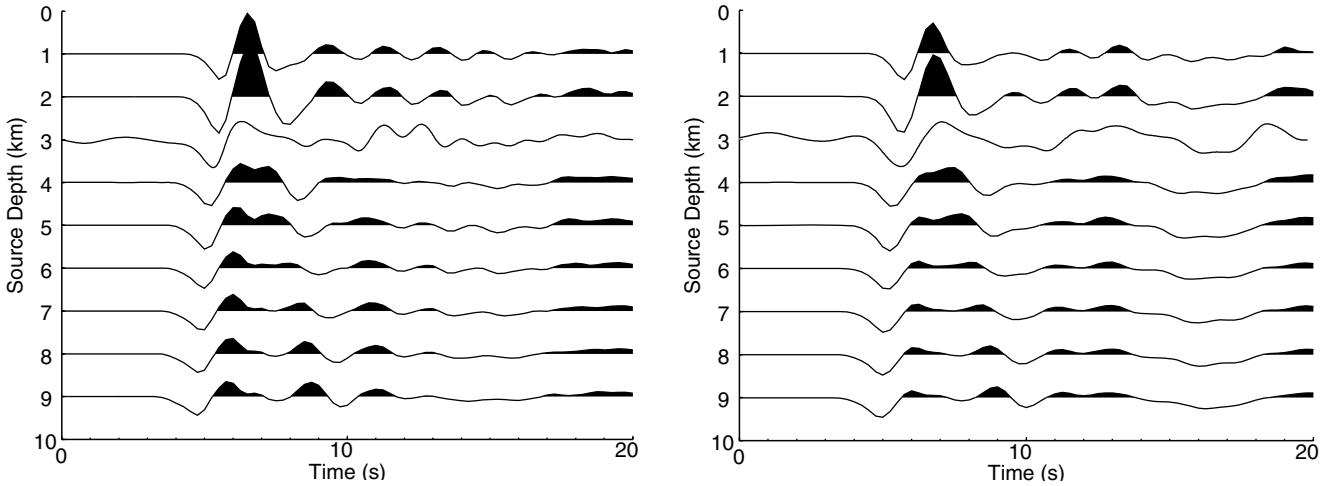

Figure 14. Observed (plotted at 3 km depth) and modelled *P*-wave group seismograms at station WOL, 147 km from the epicenter for vertical (left) and radial (right) components of ground displacement.

Variscan front coinciding with the Grande Faille du Midi (Bouroz, 1962) in southern England that places it within the Dinant zone rather than to the north of it. Aligning the Variscan front with the Bobbing-Brabourne Anticline instead might resolve these problems. Further south in the Straits a seismic profile shows deep reflectors associated with the Variscan front at its southwestern end (Brewer, 1984) that probably penetrate downward to the southwest to at least about 10 km and are most likely present as far northeast as the southern limit of the epicentral error ellipse. They are probably linked up-dip to more steeply dipping upper sections of faults (e.g., Sangatte fault).

We have determined the magnitude of the mainshock in three different ways giving an M_L 4.3, an M_w 4.0 from moment tensor inversion, and an M_w 3.8 from spectral analysis. The mismatch of the three is not very significant. The difference between the two moment magnitudes can be explained by differences in the correction for attenuation. The M_L value is determined using the scale for California because that is the default used in the United Kingdom at present, and thus, makes the value comparable to other United Kingdom earthquakes. The magnitudes for the aftershocks are calculated under the assumption that they are collocated with the mainshock. Their magnitude range is M_L 0.8–1.7. The largest aftershock is thus 2.6 magnitude units smaller than the mainshock. The corner frequency was determined for the mainshock and we derived a stress drop of 28.6 bars and a source radius of 0.5 km. The stress drop is lower than values observed from intraplate earthquakes elsewhere of about 100 bars (Lay and Wallace, 1995; Atkinson and Boore, 2006).

The PGA observed from the mainshock of 0.1g is the largest ever recorded from an earthquake in the United Kingdom. While this acceleration level was only maintained for a very short time, it seems sufficient to explain the damage observed in Folkestone. Considering a hypocenter depth of 5 km and the error ellipse around the epicenter, the distance between the source and the TFO site is between 5 and 8 km. The distance range between the source and the Foord district of Folkestone, where most damage was observed, is similar, and we can assume that PGA may have been as large here as observed at TFO. Applying the H/V method to microtremor recordings at TFO we find significant site amplification at resonant frequencies of 0.4 and 3.9 Hz. Another less significant peak at 17 Hz may have contributed to the PGA of 0.1g at a frequency of 14.3 Hz. While the site conditions in Folkestone will be somewhat different from TFO, the geology is similar enough to suggest that site amplification has contributed to the observed damage.

Conclusions

We analyzed a large amount of data from very short distances of only a few kilometers to regional and teleseismic distances to understand the source of the M_w 4.0 earthquake in Folkestone, southeastern England. Using a number of standard techniques we were able to demonstrate that the main source parameters can be determined within the associated uncertainties for a relatively small earthquake. Our main results can be summarized as follows:

- The epicenter location was 51.102°N ± 4.6 km and 1.169°E ± 6.1 km with an origin time of 07:18:11.4 (UTC). The error ellipse covers most of Folkestone. The nearest station TFO was 2 km from this epicenter.
- The hypocentral depth was 5 ± 2 km, best determined through local travel-time inversion and teleseismic depth phase modelling. Moment tensor inversion and regional phase modelling resulted in slightly more shallow depths.
- The focal mechanism was determined through moment tensor inversion of regional waveform data. The solution for a source depth of 3 km is strike = 326°, dip = 69°, and rake = −36°, which is predominantly strike slip with a normal component.
- Aftershock data were used to determine near-surface attenuation $\kappa = 0.02$ at TFO. Relative locations of the aftershocks could not be determined, as all but the last aftershocks were recorded on the nearest station only. However, three event groups were identified through waveform cross correlation showing a range of aftershock mechanisms.
- Source parameters were determined from displacement source spectra giving a stress drop of 28.6 bars and a source radius of 0.5 km.
- H/V microtremor spectral ratios determined for TFO showed amplification at 0.4 and 3.9 Hz. It is likely that similar site amplification was partly responsible for the damage observed in Folkestone.

This earthquake has shown that minor damage to buildings can occur from relatively small earthquakes. In this case the earthquake was located only about 5 km below the town. However, site amplification probably played an important role and should be investigated in detail in Folkestone retrospectively.

Data and Resources

This study would have not been possible without the data contributed by other institutions. We acknowledge the use of data from the following institutions/networks: University of Bergen (Norway), Geological Survey of Denmark and Greenland (Denmark), Royal Netherlands Meteorological Institute, AWE (United Kingdom), German Regional Seismic Network, Royal Observatory of Belgium Seismology Section, Swiss Federal Institute of Technology Zurich, French Atomic Energy Commission Département Analyse, Surveillance, Environement, Reseau National de Surveillance Sismique, Centre national de la recherche scientifique (France), Instituto Geografico Nacional (Spain), Canadian National Date Center, and IRIS (United States). Data from European broadband stations were extracted from the Observatories and Research Facilities for the European Seismology data center. Synthetic seismograms were computed with the modelling code by

Rongjang Wang. Moment tensors were computed using the mtpackagev1.1 package developed by Douglas Dreger of the Berkeley Seismological Laboratory, and Green's functions were computed using the FKRPROG software developed by Chandan Saikia of URS. The H/V spectral ratios were calculated using the JSESAME software developed during the European Commission-funded SESAME project (Atakan *et al.*, 2004a). Many of our plots are created with the Generic Mapping Tools software (Wessel and Smith, 1998).

Acknowledgments

We appreciate discussions with Kuvvet Atakan on the spectral-ratio method. We thank Susanne Sargeant, Russ Evans, David Kerridge, and Richard Luckett for reviewing the article. Review comments by Ivan Wong and an anonymous reviewer helped to improve the manuscript. This article is published with the permission of the Executive Director of the BGS (Natural Environment Research Council).

References

Abercrombie, R. E. (1997). Near-surface attenuation and site effects from comparison of surface and deep borehole recordings, *Bull. Seismol. Soc. Am.* **87,** 731–744.

Aki, K. (1967). Scaling law of seismic spectrum, *J. Geophys. Res.* **72,** 1217–1231.

Atakan, K., P.-Y. Bard, F. Kind, B. Moreno, P. Roquette, and A. TentoThe SESAME-team (2004a). J-SESAME: A standardized software solution for the H/V spectral ratio technique, *Proceedings of the 13th World Conference on Earthquake Engineering*, Vancouver, Canada, August 1–6, 2004, paper no. 2270.

Atakan, K., A.-M. Duval, N. Theodulidis, B. Guillier, J.-L. Chatelain, and P.-Y. BardThe SESAME-team (2004b). The H/V spectral ratio technique: Experimental conditions, data processing and empirical reliability assessment, *Proceedings of the 13th World Conference on Earthquake Engineering*, Vancouver, Canada, August 1–6, 2004, paper no. 2268.

Atkinson, G. M., and D. M. Boore (2006). Earthquake Ground-Motion Prediction Equations for Eastern North America, *Bull. Seismol. Soc. Am.* **96,** 2181–2205.

Auffret, J.-P., and J.-P. Colbeaux (1977). Etude structurale du Boulonnais et de son pro-longement sous-marin en Manche orientale, *Bull. Soc. Geol. Fr.* **19,** 1047–1055.

Baptie, B., L. Ottemoller, S. Sargeant, G. Ford, and A. O'Mongain (2005). The Dudley earthquake of 2002: A moderate sized earthquake in the UK, *Tectonophysics* **401,** 1–22.

Bassin, C., G. Laske, and G. Masters (2000). The Current Limits of Resolution for Surface Wave Tomography in North America, *EOS* **81,** F897.

Booth, D., J. Bott, and A. O'Mongain (2001). The UK seismic velocity model for earthquake location—a baseline review, *Internal Report IR/01/188*, British Geological Survey, Edinburgh, United Kingdom.

Bouroz, A. (1962). Contribution a l'etude de la structure du basin houiller du Boulonnais, *Ann. Soc. Geol. Nord* **82,** 27–37.

Braunmiller, J., U. Kradolfer, M. Baer, and D. Giardini (2002). Regional moment tensor determination in the European-Mediterranean area—initial results, *Tectonophysics* **356,** 5–22.

Brewer, J. A. (1984). Clues to the deep structure of the European Variscides from crustal seismic profiling in North America, in *Variscan Tectonics of the North Atlantic Region*, D. H. W. Hutton and D. J. Sanderson (Editors), Vol. **14**, Geological Society, London, United Kingdom, 253–263.

BRGM (1971). Carte geologique detaille de la France, *Technical Report.*

Brune, J. N. (1970). Tectonic stress and the spectra of seismic shear waves from earthquakes, *J. Geophys. Res.* **75,** 4997–5009.

Dahm, T., F. Kruger, K. Stammler, K. Klinge, R. Kind, K. Wygella, and J. Grasso (2007). The 2004 M_w 4.4 Rotenburg, Northern Germany earthquake, and its possible relationship with gas recovery, *Bull. Seismol. Soc. Am.* **97,** 691–704.

Davenport, C., P. Ringrose, A. Becker, P. Hancock, and C. Fenton (1989). Geological investigations of late and post glacial earthquake activity in Scotland, in S. Gregersen and P. W. Basham (Editors), *Earthquakes at North-Atlantic passive margins: Neotectonics and Postglacial Rebound*, Vol. **266**, Kluwer Academic Publications, Dordrecht, NATO ASI Series, 175–194.

Dines, H. G. (1933). The sequence and structure of the Kent Coalfield, *Summary of Progress of the Geological Survey for 1932*.

Dreger, D. S. (2003). TDMTINV: Time Domain Seismic Moment Tensor INVersion, in W. H. K. Lee, H. Kanamori, P. C. Jennings and C. Kisslinger (Editors), *International Handbook of Earthquake and Engineering Seismology*, Vol. **81B**, IASPEI, Academic Press, 1627 pp.

Engdahl, E. R., R. van der Hilst, and R. Buland (1998). Global teleseismic earthquake relocation with improved traveltimes and procedures for depth determination, *Bull. Seismol. Soc. Am.* **88,** 772–743.

Herrmann, R. (1996). Computer programs in seismology, *Technical Report*, Saint Louis University.

Hutton, L. K., and D. Boore (1987). The Ml scale in Southern California, *Bull. Seismol. Soc. Am.* **77,** 2074–2094.

Jost, M. L., and R. B. Herrmann (1989). A Student's guide and review of moment tensors, *Seis. Res. Lett.* **60,** 37–57.

Kind, R. (1979). Observation of *sPn* from the Swabian Alb earthquakes at the GRF array, *J. Geophys. Res.* **45,** 337–340.

Konno, K., and T. Ohmachi (1998). Ground-motion characteristics estimated from spectral ratio between horizontal and vertical components of microtremor, *Bull. Seismol. Soc. Am.* **88,** 228–241.

Lamplugh, G. W., F. L. Kitchin, and J. Pringle (1923). The concealed Mesozoic rocks in Kent, in *Memoir of the Geological Survey (England and Wales)*, Geological Survey, United Kingdom.

Lay, T., and T. C. Wallace (1995). *Modern Global Seismology*, Academic Press, San Diego, California.

Lienert, B. R. (1994). HYPOCENTER 3.2: A computer program for locating earthquakes locally, regionally and globally, Technical Rept., Hawaii Institute of Geophysics and Planetology, Honolulu.

Lienert, B. R. E., and J. Havskov (1995). A computer program for locating earthquakes both locally and globally, *Seis. Res. Lett.* **66,** 26–36.

Melville, C. P., A. Levert, P. Alexandre, J. Lambert, and J. Vogt (1996). Historical seismicity of the Strait of Dover—Pas de Calais, *Terra Nova* **8,** 626–647.

Minguely, B., J.-L. Mansy, M. Everaerts, G. M. Manby, and O. Averbuch (2005). Geophysical modelling as an aid to understanding the structure of the Dover Straits, *Comptes Rendus Geosci.* **337,** 305–313.

Mooney, W., G. Laske, and G. Masters (1998). Crust 5.1: A global crustal model at 5 × 5degrees, *J. Geophys. Res.* **103,** 727–747.

Musson, R. M. W. (1994). A catalogue of British earthquakes, Technical Rept., British Geological Survey.

Nafe, J. E., and C. L. Drake (1963). Physical properties of marine sediments, in M. N. Hill (Editor), *The Sea*, Vol. **3**, Interscience, New York, 794–815.

Nakamura, Y. (1989). A method for dynamic characteristics estimation of subsurface using microtremor on the ground surface, *QR RTRI* **30,** 25–33.

Noghoshi, M., and T. Igarashi (1970). On the propagation characteristics of microtremors, *J. Seismol. Soc. Japan* **23,** 264–280, (in Japanese with English abstract).

Noghoshi, M., and T. Igarashi (1971). On the amplitude characteristics of microtremors, *J. Seismol. Soc. Japan* **24,** 24–40, (in Japanese with English abstract).

Ottemöller, L., and L. G. Evers (2008). Seismo-acoustic analysis of the Buncefield oil depot explosion in the UK, 11 December 2005, *Geophys. J. Int.* **172,** 1123–1134.

Ottemöller, L., and J. Havskov (2003). Moment magnitude determination for local and regional earthquakes based on source spectra, *Bull. Seismol. Soc. Am.* **93,** 203–214.

Ottemöller, L., H. H. Nielsen, K. Atakan, J. Braunmiller, and J. Havskov (2005). The 7 May 2001 induced seismic event in the Ekofisk oil field, North Sea, *J. Geophys. Res.* **110,** B10301, doi 10.1029/2004JB003374.

Plumptre, J. H. (1959). Underground waters of the Kent Coalfield, *Trans. Inst. Min. Eng.* **119,** 155–169.

Sargeant, S. L., P. Stafford, R. Lawley, G. Weatherill, A.-J. S. Weston, J. Bommer, P. Burton, M. Free, R. M. W. Musson, A. Kuuyuor, and T. Rossetto (2008). The felt effects of the Folkestone (UK) earthquake of 28 April 2007 (4.2 ML), *Seis. Res. Lett.* **79,** 672–687.

SESAME (2004). Guidelines for the implementation of the H/V spectral ratio technique on ambient vibrations—measurements, processing and interpretation, *SESAME European Research Project WP12 Deliverable D23.12, Technical Report*, European Commission Research General Directorate Project No. EVG1-CT-2000-00026 SESAME.

Shapiro, N. M., and M. H. Ritzwoller (2002). Monte-Carlo inversion for a global shear velocity model of the crust and upper mantle, *Geophys. J. Int.* **151,** 88–105.

Shephard-Thorn, E. R., R. D. Lake, and E. A. Atitullah (1972). Basement control of structures in the Mesozoic rocks in the Strait of Dover region, and its reflection in certain features of the present land and submarine topography, *Philos. Trans. R. Soc. London* **272A,** 99–110.

Singh, S. K., R. J. Apsel, J. Fried, and J. N. Brune (1982). Spectral attenuation of *SH* waves along the Imperial fault, *Bull. Seismol. Soc. Am.* **72,** 2003–2016.

Smith, N. J. P., J. D. Cornwell, S. Holloway, and R. A. Edwards (2001). High velocity layer beneath seismic 'reflector X' in the Bristol Channel may be Carboniferous Limestone: Implications for a possible Exmoor-Cannington Park thrust: Reply to Brooks and Miliorizos, *Proc. Ussher Soc.* **12,** 241–242.

Sørensen, M. B., I. Oprsal, S. Bonnefoy-Claudet, K. Atakan, P. M. Mai, N. Pulido, and C. Yalciner (2006). Local site effects in Ataköy, Istanbul, Turkey, due to a future large earthquake in the Marmara Sea, *Geophys. J. Int.* **167,** 1413–1424, doi 10.1111/j.1365-246X.2006.03204.x.

Wang, R., and H. Wang (2007). A fast converging and anti-aliasing algorithm for Green's functions in terms of spherical or cylindrical harmonics, *Geophys. J. Int.* **170,** 239–248.

Warren, S. T., and C. S. Harris (1996). An interpretation of the structural geology, in *Engineering Geology of the Channel Tunnel*, C. S. Harris, M. B. Hart, P. M. Varley and C. D. Warren (Editors), Thomas Telford Ltd, 421–435.

Wessel, P., and W. H. F. Smith (1998). New, improved version of the Generic Mapping Tools released, *EOS Trans. AGU* **79,** 579.

British Geological Survey
Murchison House, West Mains Road
Edinburgh, EH9 3LA, United Kingdom
lot@bgs.ac.uk
(L.O., B.B.)

British Geological Survey
Kingsley Durham Center
Nottingham, NG12 5GG, United Kingdom
(N.J.P.S.)

Manuscript received 27 February 2008